Journal of Materials Chemistry A

Efficient Removal of Short-Chain and Long-Chain PFAS by Cationic Nanocellulose

Journal:	*Journal of Materials Chemistry A*
Manuscript ID	TA-ART-03-2023-001851.R1
Article Type:	Paper
Date Submitted by the Author:	16-Apr-2023
Complete List of Authors:	Li, Duning; Stony Brook University The State University of New York, Chemistry Lee, Cheng-Shiuan; Academia Sinica, Research Center for Environmental Changes; Stony Brook University, Center for Clean Water Technology Zhang, Yi; New York State Center for Clean Water Technology, Stony Brook University Das, Rasel; Stony Brook University, Department of Chemistry Akter, Fahmida; Stony Brook University, Chemistry Venkatesan, Arjun; Stony Brook University, Civil Engineering Hsiao, Benjamin; Stony Brook University, Department of Chemistry

Efficient Removal of Short-Chain and Long-Chain PFAS by Cationic Nanocellulose

Duning Li[1], Cheng-Shiuan Lee[2,3], Yi Zhang[2], Rasel Das[1], Fahmida Akter[1], Arjun K. Venkatesan[2,4,*], and Benjamin S. Hsiao[1,*]

[1]Department of Chemistry, Stony Brook University, Stony Brook, NY 11790, USA

[2]New York State Center for Clean Water Technology, Stony Brook University, Stony Brook, NY 11794, USA

[3]Research Center for Environmental Changes, Academia Sinica, Taipei 115, Taiwan

[4]School of Marine and Atmospheric Sciences, Stony Brook University, Stony Brook, NY 11794, USA

[*]Corresponding authors:

Email address: arjun.venkatesan@stonybrook.edu (A. K. Venkatesan), benjamin.hsiao@stonybrook.edu (B. S. Hsiao)

Abstract

Although most manufacturers stopped using long-chain per- and polyfluoroalkyl substances (PFASs), including perfluorooctanoic acid (PFOA) and perfluorooctanesulfonic acid (PFOS), short-chain PFASs are still widely employed. Short-chain PFASs are less known in terms of toxicity and have different adsorption behavior from long-chain PFASs. Previous studies have shown electrostatic interaction with the adsorbent to be the dominant mechanism for the removal of short-chain PFASs. In this study, we designed a high charge density cationic quaternized nanocellulose (QNC) to enhance the removal of both short- and long-chain PFASs from contaminated water. Systematic batch adsorption tests were conducted using the QNC adsorbent to compare its efficiency against PFASs with varying chain lengths and functional groups. From the kinetic study, PFBA (perfluorobutanoic acid), PFBS (perfluorobutanesulfonic acid) and PFOS showed rapid adsorption rates, which reached near equilibrium values (> 95 % of removal) between 1 min to 15 min, while PFOA required a relatively longer equilibration time of 2 h (it obtained 90 % of removal within 15 min). According to the isotherm results, the maximum adsorption capacity (Q_m) of the QNC adsorbent exhibited the following trend: PFOS (Q_m = 559 mg/g or 1.12 mmol/g) > PFOA (Q_m = 405 mg/g or 0.98 mmol/g) > PFBS (Q_m = 319 mg/g or 1.06 mmol/g) > PFBA (Q_m = 121 mg/g or 0.57 mmol/g). This adsorption order generally matches the hydrophobicity trend among four PFASs associated with both PFAS chain length and functional group. In competitive studies, pre-adsorbed short-chain PFASs were quickly desorbed by long-chain PFASs, suggesting that the hydrophobicity of the molecule played an important role in the adsorption process on to QNC. Finally, the developed QNC adsorbent was tested to treat PFAS-contaminated groundwater, which showed excellent removal efficiency (>95%) for long-chain

PFASs (C7–C9) even at a low adsorbent dose of 32 mg/L. However, short-chain PFASs (i.e., PFBA and perfluoropentanoic acid (PFPeA)) were poorly removed by the QNC adsorbent (0% and 10% removal, respectively) due to competing constituents in the groundwater matrix. This was further confirmed by controlled experiments that revealed a drop in the performance of QNC to remove short-chain PFASs at elevated ionic strength (NaCl), but not for long-chain PFASs, likely due to charge neutralization of the anionic functional group of PFASs by inorganic cations. Overall, the QNC adsorbent featured improved PFAS adsorption capacity at almost two-fold of PFAS removal by granular activated carbons, especially for short-chain PFASs. We believe, QNC can complement the use of common treatment methods such as activated carbon or ionic exchange resin to remove a wide range of PFAS pollutants, heading towards the complete remediation of PFAS contamination.

Keywords: Cationic adsorbent, quaternized nanocellulose, PFAS, adsorption.

1. Introduction

Per- and polyfluoroalkyl substances (PFASs) have been extensively used in various industrial products, such as polymer additives and surfactants, since the 1940s.[1] Due to the presence of multiple strong carbon-fluorine (C-F) bonds, PFASs exhibit high stability and persist in the environment without degradation. Consequently, the issue of PFAS pollution has exacerbated rapidly, and the need to develop effective remediation methods to remove these compounds has caught public and scientific attention. According to a 2019 Environmental Protection Agency (EPA) report, as many as 110 million people may have been exposed to PFAS-contaminated drinking water.[2] Short-chain PFASs are currently abundant in commerce as they serve as replacement chemicals for phased out long-chain? PFASs.[3] Short-chain PFASs are defined as molecules with shorter number of C-F units (C ≤6 for perfluorinated carboxylic acids and C ≤5 for sulfonic acids).[4] Their properties are yet to be fully understood and their effective removal strategies and efficiency are only scarcely reported.[5] A recent report indicates that many fast food packaging materials contain a significant amount of total organic fluorine (larger than 100 mg/L) with perfluorobutanoic acid (PFBA) having the highest concentration (among 30 PFAS targeted compounds tested).[6] In another report, ~~was also thought that~~ the existence of short-chain PFASs is thought to have possible linkage with COVID-19 complications.[7] Several short-chain PFASs, such as perfluorobutane sulfonate (PFBS) and perfluorohexanoate (PFHxA), have already been shown to possess potential reproductive toxicity,[8] and some PFAS precursors and alternative PFASs including perfluorooctane sulfonamide (FOSA) and hexafluoropropylene oxide dimer acid (HFPO-DA) may also affect gene expression and alter drug metabolism.[9]

85 Among the many remediation methods demonstrated, adsorption is the simplest and most
86 cost-effective approach to remove PFASs. This is because other remediation methods, such as
87 electrochemical oxidation or electron beam, capable of destroying/degrading the PFAS
88 components,[10] require complex instrumental setup and intensive energy consumption.[11] The
89 incomplete destruction process by these methods can also produce short-chain PFASs that remain
90 harmful.[12] Unfortunately, common sorptive materials, such as granular activated carbon (GAC),
91 although suitable to treat hydrophobic and long chain PFASs, exhibit early breakthrough and only
92 mediocre adsorption efficiency for short-chain PFASs.[13] The reason is that short-chain PFASs
93 behave less like surfactants and are ineffectively removed by hydrophobic interaction. [14, 15] To deal
94 with this, modification of adsorbents with proper cationic functional groups that can provide
95 electrostatic interaction with short-chain PFASs becomes a potential approach. There have been
96 several new sorptive nanomaterials developed that can remove short-chain PFASs with improved
97 efficiency. For example, carbon nanotube (CNT), graphene, zeolites, inorganic metallic
98 nanoparticles, and their composites have been used to remove short-chain PFASs from wastewater
99 and groundwater with some success.[15, 16] However, these nanomaterials are not eco-friendly due
100 to their adverse toxicity and possible leaching and they are expensive to manufacture.[17] Therefore,
101 there is a need to develop low cost, environmentally friendly and effective nanomaterials, such as
102 nanocellulose-based systems,[18] for PFAS removal.
103
104 Cellulose is the most abundant biopolymer on Earth. Functionalized cellulose-based
105 adsorbents from cheap feedstocks with low toxicity and biocompatibility are broadly used in many
106 practical water purification treatments.[18] However, very limited studies have been reported for
107 PFAS remediation using cellulosic adsorbents.[19] To design an effective adsorbent based on the

concept of nanocellulose scaffold, we consider two primary PFAS removal mechanisms: (i) hydrophobic attraction between the scaffold and C-F chains, and (ii) electrostatic attraction between the anionic functional groups in PFASs and cationic functional sites on the scaffold. Previously, some groups suggested that electrostatic attraction is the dominant adsorption mechanism for the short-chain PFAS removal, while hydrophobicity is the dominant adsorption mechanism for the long chain PFAS removal. [3, 5, 14]

In this study, positively charged quaternized ammonium functionalized nanocellulose or quaternized nanocellulose (QNC) adsorbent was prepared to test our hypothesis that highly charged adsorbents could enhance short-chain PFAS removal. We note that similar microscale quaternized cellulose (QC) adsorbents have been reported for long-chain PFAS removal,[20] but the efficacy in QNC (with a significantly higher surface area than QC) for short-chain PFAS removal has yet to be reported. The specific objectives of this study were to: (i) use wood pulp as starting material to synthesize nanoscale QNC through one-step quaternization method, where its degree of functionalization could be adjusted by the etherification process; (ii) evaluate the removal performance of QNC using four model PFASs (perfluorooctanesulfonic acid (PFOS), perfluorooctanoic acid (PFOA), PFBS and PFBA) with different chain length (long-chain: C8; short-chain: C4) and charged functional groups (sulfonate and carboxylate) in the targeted contaminants, (iii) probe the mechanisms on PFAS uptake by QNC in the batch system using sorption isotherm and kinetics models; and (iv) further explore the removal mechanisms and understand the effects from different C-F tail lengths and functional groups in PFASs by applying competitive adsorption studies and groundwater tests. We observed that QNC exhibited stronger affinity towards long-chain and sulfonated PFASs compared to short-chain and carboxylated

131 PFASs. The current study confirmed that electrostatic interaction is the major removal mechanism
132 of PFAS by the QNC system, while its hydrophobicity also adds to the adsorption process,
133 resulting in higher adsorption capacity for long-chain PFASs.
134
135 **2. Experimental Methods**
136
137 **2.1. Materials**
138
139 Never-dried bleached wood pulp was obtained from Domsjo Fabriker, Sweden. The pulp
140 exhibited the hemicellulose content of 4.5% (w/w) and lignin content of 0.6% (w/w) as measured
141 by the R18 test (pulp samples treated with 18% NaOH to dissolve the pulp impurities). Sodium
142 hydroxide (Pellet) was purchased from Macron Fine Chemicals (ACS reagent grade).
143 Hydrochloric acid (36.5-38%) was purchased from VWR Chemical (ACS reagent grade).
144 Glycidyltrimethylammonium chloride (GTMAC) (≥ 90%), silver nitrate (≥ 99.0%),
145 heptadecafluorooctanesulfonic acid potassium salt (PFOSK) (≥ 98.0%), nonafluorobutanesulfonic
146 acid (PFBS) (≥ 97.0%), and heptafluorobutyric acid (PFBA) (≥ 98.0%) were purchased from
147 Sigma-Aldrich (USA) (analytical or reagent grade). Pentadecafluorooctanoic acid (PFOA)
148 (>98.0%) was purchased from TCI America. Isotopically labeled PFAS internal standards, $^{13}C_4$-
149 PFBA, $^{13}C_3$-PFBS, $^{13}C_8$-PFOA, and $^{13}C_8$-PFOS, were purchased from Wellington Laboratories
150 (Guelph, Ontario). LC-MS grade methanol was purchased from Honeywell, USA. Regenerated
151 cellulose syringe filter (pore size of 0.2 um) was purchased from Corning Inc. USA, where a
152 preliminary study was carried out to confirm that there was no filter loss or PFAS releasing.
153 Deionized water was used in all the experiments for preparation of reagents and experimental

154 procedures. PFAS contaminated groundwater samples were collected on Long Island, NY. The
155 water quality parameters and background PFAS concentrations in the Long Island groundwater
156 are shown in Table S1 and S2, respectively (*Supporting Information*).
157
158 **2.2. Preparation of Quaternized Nanocellulose (QNC)**
159
160 The synthesized procedure to prepare QNC was revised from earlier studies.[21-23] In brief,
161 10 g of never-dried wood pulp was mixed with a certain amount of NaOH solution and DI water
162 to achieve the NaOH concentration of 5 wt% and the cellulose fiber suspension at 2.5 wt% or 7.5
163 wt%. After 30 min stirring at room temperature, GTMAC (glycidyltrimethylammonium chloride)
164 was added at the ratio of 9:1 or 12:1 mol/mol AGU (anhydroglucose unit) as shown in Table 1.
165 The reaction took place at 65°C for 8 h. To quench the reaction, HCl was added dropwise into the
166 final suspension to neutralize the excess base. Vacuum filtration was used to isolate the reaction
167 mixture, which was washed with DI water several times until the pH became 7.0 to obtain QC. To
168 obtain QNC, around 400 ml 0.3 % (w/v) QC suspension in DI water was subjected to GEA Niro
169 Soavi Panada Plus homogenizer at 300 bar for 5 cycles.
170
171 **Table 1.** Preparation of different QNC adsorbents and their functional group contents.

Sample	Reaction conditions	GTMAC added amount (mol/mol AGU)	Trimethylammonium chloride content
Raw wood pulp	Unmodified biomass	N.A.	N.A.

QNC 9:1-a	2.5 wt% wood pulp with 5 wt% NaOH at 65 ℃ for 8 h	9:1	0.327 mmol/g
QNC 9:1-b	7.5 wt% wood pulp with 5 wt% NaOH at 65 ℃ for 8 h	9:1	0.341 mmol/g
QNC 12:1	7.5 wt% wood pulp with 5 wt% NaOH at 65 ℃ for 8 h	12:1	0.486 mmol/g

172

173 **2.3. Characterization Methods**

174

175 Fourier-Transform Infrared Spectroscopy (FTIR) was used to investigate the functional
176 groups and chemical bonds on cellulose materials (Text S1). The crystallinity information was
177 obtained from X-Ray Diffraction (XRD) (Text S2). Conductivity titration (Text S3), zeta potential
178 measurement (Text S4) and BET surface area measurement (Text S5) further characterized the
179 degree of functionalization, charge density and surface area for QNC adsorbent, respectively. To
180 observe and confirm the nanofibrous structure, scanning electron microscope (SEM) and
181 transmission electron microscope (TEM) were also performed to estimate the fiber size and
182 dimension (Text S6). Details of instrumental information and sample preparation could be found
183 in supporting information.

184

185 **2.4. PFAS Adsorption Experiment**

186

187 Adsorption experiments were conducted to determine the PFAS removal efficiency using
188 the QNC 12:1 sample (in a gel form at the chosen concentration, Table 1), since this sample
189 contained the highest charge density. Although we considered QNC as an adsorbent, it works more

190 like a coagulant. The presence of QNC suspension/gel (depending on the concentration) can
191 neutralize the negatively charged PFAS molecules and form large aggregates or flocs with strong
192 gel property. In specific, we observed the formation of white flocs after mixing QNC with high
193 concentration of PFAS. These flocs containing PFAS can be efficiently removed from water by
194 conventional low energy microfiltration approaches (e.g., through gravity).
195
196 In the kinetic study, an appropriate amount of PFAS solution (5 mg PFAS/L in mg/L) was
197 mixed with the QNC gel (320 mg/L for PFBA/PFBS, and 32 mg/L for PFOA/PFOS) in each
198 experimental vial. The PFAS solution and the QNC gel were well mixed in an orbital shaker
199 operated at 150 rpm, where a small aliquot of sample was taken at different time points from 1
200 min to 24 h for measurement. In the isotherm study, PFAS solutions with varying initial
201 concentrations (1–50 mg/L for PFOA and PFOS; 1–100 mg/L for PFBA; 1–250 mg/L for PFBS)
202 were measured with the QNC gel at 32 mg/L (for PFOA and PFOS) or 320 mg/L (PFBA and
203 PFBS). The adsorbent dose in the isotherm study is the same as that in the kinetic study for each
204 PFAS, where the adsorption time was set as 24 h to make certain that the equilibrium was fully
205 reached. In the competition study, bisolute systems with either PFOS+PFBS or PFOA+PFBA were
206 tested. The initial concentration of PFAS was about 60 mg/L and the QNC gel concentration was
207 160 mg/L. In the displacement study, 60 mg/L of PFBA or PFBS was mixed with 160 mg/L of
208 QNC gel first and allowed to equilibrate. After 24 h, equal concentration of PFOA or PFOS was
209 spiked into the system. In the ion test, 0.1 M and 1 mM NaCl solutions were added to the
210 QNC/PFAS system separately. PFAS concentrations were set as 2 mg/L for PFOS/PFOA with 32
211 mg/L QNC, and 10 mg/L for PFBS/PFBA with 320 mg/L QNC (similar to the condition in kinetic
212 study). For the groundwater treatment, increasing dose of QNC gel was added ranging from 32

mg/L to 640 mg/L, where the adsorption time was set at 1 h. The pH value was measured as between 3 and 4 for the kinetic, isotherm and competition studies in DI water after adding PFAS, and at 7 for the groundwater adsorption test. A 0.2-μm regenerated cellulose (RC) syringe filter was used to remove all adsorbents after the adsorption study. Control experiments were carried out to confirm that the filter loss of different PFAS on RC filter was negligible.

The filtrate was diluted 1,000x or 10,000x with LC-MS grade methanol, and then spiked with isotopically labeled PFAS internal standards (Table S3, *Supporting Information*) prior to LC-MS/MS analysis. The adsorption experiments were carried out twice to determine the average value and deviation.

2.5. PFAS Analysis

PFAS quantification was performed using an Agilent 6495B liquid chromatography tandem mass spectrometer (LC-MS/MS). The analytical column was Zobrax Eclipse Plus C18 (50 x 3 mm, 1.8 μm) (Agilent, Santa Clara, CA) and a delay column (Agilent Zobrax Eclipse Plus, 50 x 4.6 mm, 3.5 μm) was placed between the pump and the multi-sampler to minimize any background contamination from solvent, tubing, and pump parts. The aqueous phase was 5 mM ammonium acetate solution (A) and the organic phase was 100% methanol (B). The flow rate was maintained at 0.4 mL/min throughout the run and the injection volume was 5 μL. The initial solvent gradient was set at 90% A and 10% B and maintained for 30 s. The gradient was then ramped from 10% B to 30 % B ~~in~~ at 2 min, and then further ramped from 30% B to 95% B ~~in~~ at 12 min. At the end, the solvent composition was switched to 95% A and equilibrated for 6 min prior to the next

236 injection. Detailed LC-MS/MS operating conditions and corresponding parameters are listed in
237 Table S3 (*Supporting Information*). All samples were analyzed in electrospray ionization negative
238 (ESI-) mode and data was acquired in a multiple reaction monitoring (MRM) acquisition mode.
239 Two transitions (quantifier and qualifier) were monitored for each PFAS compound except for
240 PFBA (Table S4, *Supporting Information*). Agilent MassHunter Quantitative Analysis (B.09.00)
241 was used for data processing.
242
243 **3. Results and Discussion**
244
245 **3.1. Characterizations of Quaternized Nanocellulose**
246
247 Following the green chemistry principle, we used the quaternization modification method
248 to create cationic QNC adsorbents due to its simplicity (i.e., one-pot reaction), less chemical load,
249 and aquatic reaction conditions at a mild temperature. The approach has a good potential to achieve
250 sustainability in producing effective remediations materials with low cost and low toxicity for
251 PFAS removal. To understand the possible optimization pathway for the quaternization
252 modification, we tested two cellulose concentrations: diluted (2.5 wt%) and concentrated (7.5
253 wt%). Previous studies indicated that there are a few key factors affecting the degree of
254 quaternization, including NaOH concentration and GTMAC addition amount.[22, 23] It has been
255 reported that the hydroxyl groups on the cellulose surface should be activated by hydroxide ions
256 in order to initiate the nucleophilic addition, in which 5 wt% of NaOH was found to be an
257 appropriate condition to achieve this.[23] If the NaOH concentration is too high, the native cellulose
258 structure can be changed (crystalline conversion can take place). Additionally, the degree of

quaternization has been found to be positively correlated with the added GTMAC amount. However, if too much GTMAC is added, the reaction can produce amorphous cellulose derivates and destruct the microfibril structure.[22, 23] Another side reaction is the hydrolysis of GTMAC, which can yield non-reactive reagent and thus decrease the degree of substitution.[24] The resulting QNC samples and corresponding characterization results are summarized in Table 1. Based on this study, we found that the QNC 12:1 sample created by the cellulose condition of 7.5 wt% and the highest GTMAC content used (12:1) created the highest cationic charge, which ~~will be~~ we used for the adsorption study in this work.

The functional groups for raw wood pulp and varying QNC samples were confirmed from the FTIR spectra. As seen in Figure 1a, all samples exhibited signature cellulose peaks at a region from 500 to 1400 cm^{-1} (e.g., the intense pyranose ether band at 1050 cm^{-1}, the broad peak between 3200 to 3500 cm^{-1} from the -OH groups of the cellulose scaffold). Most importantly, we observed that the appearance of a new peak at 1480 cm^{-1} in all QNC samples, that could be attributed to the trimethyl group of quaternary ammonium.[22] Additionally, the peak at 1640 cm^{-1} might be due to the vibration of quaternary nitrogen bond or bound water, which was seen for both QNCs and wood pulp, respectively. The peak at 2897 cm^{-1} for wood pulp fragmented into two small peaks might be due to the addition of quaternary ammonium group, which could be assigned to the out-of-plane bending of the C-H stretching in methyl group.[23] The spectra in Figure 1a indicate the successful incorporation of trimethyl quaternary ammonium groups on the cellulose backbone. Additionally, we measured the QNC sample after PFOA adsorption and compared that with the spectra of PFOA and neat QNC (Figure 1b). It was seen that a new peak appeared at 1680 cm^{-1}, which could be assigned to the amide I vibration from the CO-NH bond.[25, 26] This observation

282 supports the augment that the carboxylate group on PFOA can interact with the quaternary
283 ammonium group on QNC through electrostatic interaction.
284

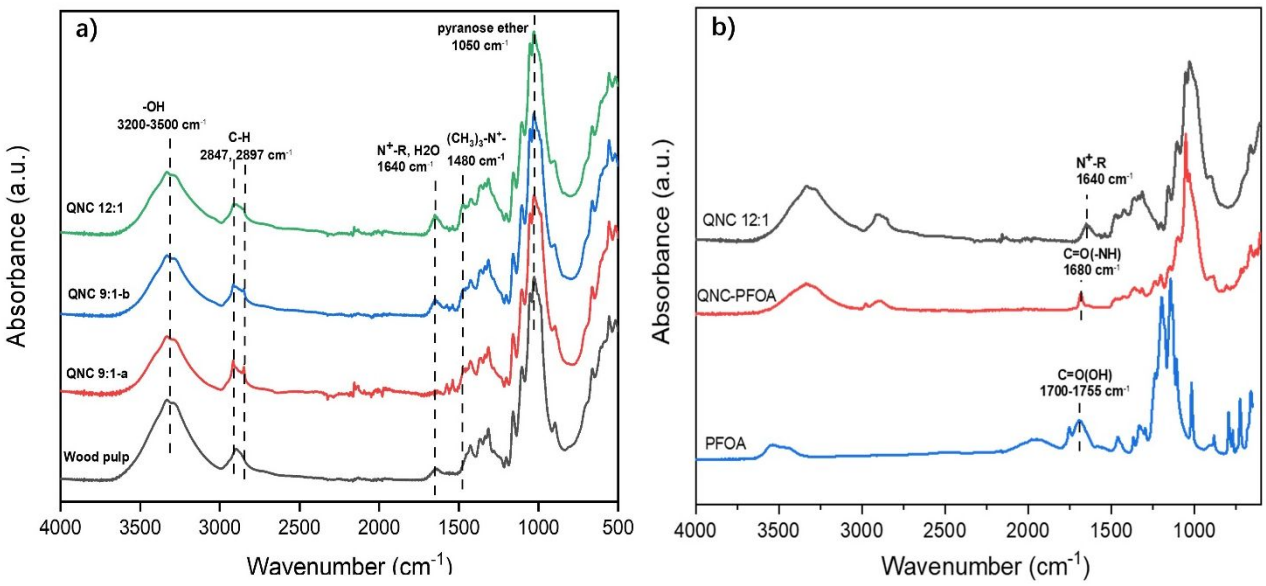

285 **Figure 1.** (a) The FTIR spectra for raw wood pulp, and three QNC samples (QNC 9:1-a, 9:1-b
286 and 12:1); (b) Comparison of QNC 12:1, ONC-PFOA and PFOA.
287

288 For the cellulose and QNC morphology analysis, we used both SEM and TEM techniques,
289 and the results are shown in Figure 2. SEM images show partially defibrillated fibers (Figures 2c
290 and 2d) for QNC 12:1 when compared with wood pulp fibers (Figures 2a and 2b). Overall, the
291 pulp fibers were thicker in size and they were interlocked with each other (Figures 2a and 2b),
292 whereas some thinner individual fibers were observed on QNC (Figures 2c and 2d). This could be
293 due to the homogenization process of QNC slurry, which resulted in defibrillation of microfibers
294 into nanofibers due to the charge repulsion. TEM images confirmed that after homogenization,
295 QNC contained mainly the nanofiber form (Figures 2ae and 2f). The average fiber dimensions of
296 QNC 12:1 measured from the TEM images were 110 ± 57 nm in length and 6.5 ±1.4 nm in width.

297 However, we noted that some part of QNC 12:1 contained partially defibrillated morphology
298 (observed as swollen microfibers). Nevertheless, the overall surface area in QNC is significantly
299 larger than that of unmodified wood pulp.
300

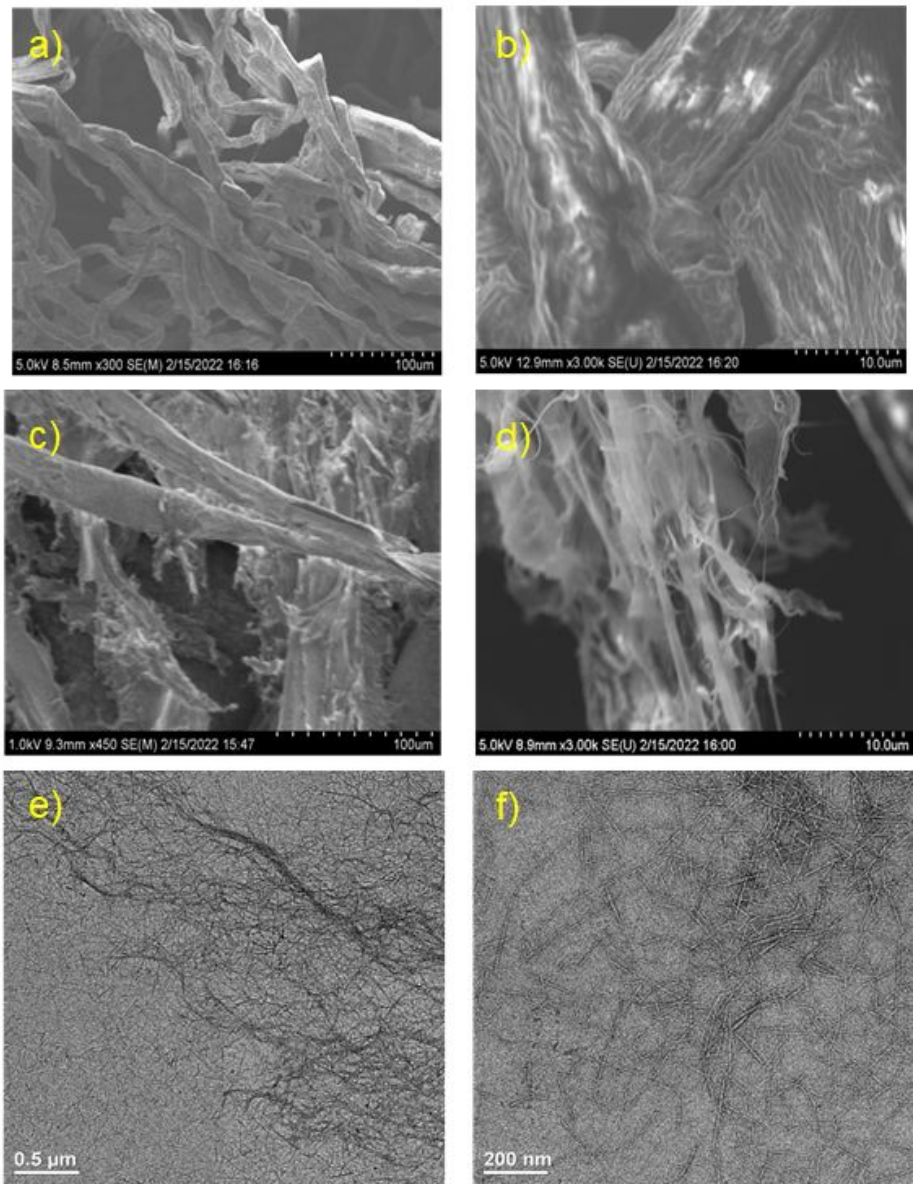

301
302 **Figure 2.** SEM images for air-dried wood pulp fiber (a and b) and freeze-dried QNC 12:1 (c and
303 d). TEM images for QNC 12:1 (e and f).
304

Conductivity titration was used to quantitatively determine the amount of quaternary ammonium groups (i.e., the trimethylammonium chloride content in Table 1) and the degree of substitution in QNC samples. Zeta potential was also performed for measuring the overall charge density for wood pulp and QNC in the slurry or suspension form. From the conductivity titration study, no quaternary ammonium groups were observed from wood pulp (its zeta potential was -20.3 mV, Table 2). In contrast, both QNC 9:1-a and QNC 9-1-b samples exhibited a relatively high quaternary ammonium content (0.327 to 0.341 mmol/g, respectively). The higher quaternary ammonium content in QNC 9-1-b might be due to the decreasing water content in the reaction. As the GTMAC ratio was increased to 12 to 1, the quaternary ammonium content increased to 0.486 mmol/g, corresponding to the degree of substitution equal to 0.078 mol/mol AGU. These data match the zeta potential results, where all QNC samples showed positive surface charges with the following order: QNC 9:1-a (27.9 mV) < QNC 9:1-b (36 mV) < QNC 12:1 (42.7 mV). Additionally, the zeta potential was also measured under different pH condition for the QNC 12:1 sample (Figure S1, *Supporting Information*). The results indicated that there was no significant change in the zeta potential value when the pH value was increased from 2 to 10. This indicates that the cationic quaternary ammonium groups in QNC remain relatively stable in a wide pH range. To understand the removal mechanism, we also performed the zeta potential measurement of QNC loaded with PFOA (Figure S2, *Supporting Information*). In this study, 1.6 mL 0.03 wt% of QNC was firstly added into the small cuvette. Subsequently, 20, 40 and 60 μl of 1g/L PFOA was mixed with the QNC suspension, respectively, for certain time to reach equilibrium. It was found that zeta potential after PFOA adsorption decreased with the PFOA content from 38 mV to 10 mV. This observation indicates that the adoption of anionic PFAS molecules neutralize the cationic groups

327 on QNC resulting in a lower surface charge of the scaffold, confirming that electrostatic interaction
328 is the major adsorption mechanism by QNC for PFAS removal.
329
330 The XRD profiles for both wood pulp and QNC samples exhibited the cellulose I crystal
331 structure (Figure S3, *Supporting Information*). These profiles displayed three major diffraction
332 peaks at 14.8°, 16.8° and 22.6°, indicating that cationization occurred mainly on the cellulose
333 surface. There is no major difference in CI between the original pulp, QNC 9:1-a and 9:1-b samples,
334 but the QNC 12:1 sample showed a lower CI value of 63% (Table 2). This observation is consistent
335 with a previous study that the use of a large amount of GTMAC could result in converting
336 crystalline microfibril structure into amorphous QNC derivatives.[22] This indicates at a lower
337 GTMAC concentration, the cationization reagent tends to react with the amorphous cellulose
338 chains first since their intermolecular force is relatively weak. As GTMAC concentration increases,
339 the reagent begins to attach the crystalline chains resulting in the decrease in total crystallinity (as
340 QNC 12:1).
341
342 **Table 2**. Characterization results for different QNC adsorbents

Sample	Crystallinity index (CI value)	Zeta potential value	BET surface area
Wood pulp	77%	-20.3 mV	6.10 m^2/g
QNC 9:1-a	77%	27.9 mV	21.62 m^2/g
QNC 9:1-b	76%	36.0 mV	72.17 m^2/g
QNC 12:1	63%	42.7 mV	50.12 m^2/g

343

344 The available surface area is an important parameter for the adsorption property. In this
345 case, the solid samples' (air-dried wood pulp fiber and freeze-dried QNC samples) surface areas
346 were measured by the BET technique, which results are shown in Table 2. It was seen that all QNC
347 samples exhibited a much higher surface area compared with wood pulp (6.09 m^2/g). The BET
348 values in varying QNC samples can be explained by the degree of fibrillation. In specific, the
349 comparison between the surface areas of QNC 9:1-a and 9:1-b indicate that the higher degree of
350 quaternization leads to greater fibrillation, as expected. Surprisingly, the QNC 12:1 exhibited a
351 lower surface area than QNC 9:1-b, which could have resulted from the excess dosage of GTMAC
352 leading to some side reaction and the possible collapse of the scaffold structure during freeze-
353 drying. We note that the surface area of QNC sample is not as high as those of solid porous
354 materials, such as organosilica or GAC (average 400 - 600 m^2/g).[27, 28] Again, this may reflect the
355 fact that even with the freeze-drying technique, some nanocellulose scaffold may still collapse,
356 resulting in a tighter porous network structure.
357
358 **3.2. Batch Adsorption Studies for PFAS Removal**
359
360 **3.2.1. Adsorption Kinetics**
361
362 The kinetic adsorption study was performed to evaluate the adsorption rate of different
363 PFASs using the QNC 12:1 adsorbent (referred as QNC adsorbent hereinafter), where the results
364 are shown in Figure 3 (also Tables S5 (a)-(d), *Supporting Information*). In Figure 3(a), it was seen
365 that the adsorption equilibrium was achieved within 2 h for PFOA. In contrast, a significantly
366 faster adsorption rate (99% removal within one minute) was observed for PFOS (Figure 3c). For

short-chain PFBA and PFBS, a relatively fast equilibrium (within 15 minutes) was also observed. However, sorption fluctuations were seen in the first two hours (Figures 3b and 3d). These fluctuations are likely caused by the quasistatic sorption-desorption equilibrium between the weakly bonded short-chain PFAS and QNC in the initial sorption phase.[29]

Both pseudo-first order (Eq. 2) and pseudo-second order (Eq. 3) kinetic models were used to fit the kinetic data, where the fitting parameters are listed in Table 3. The expressions of these two models are as follow:[28, 30]

$$\ln\left(q_{e,exp} - q_t\right) = \ln q_{e,cal} - k_1 t \quad (1)$$

$$\frac{t}{q_t} = \frac{1}{k_2 q_e^2} + \frac{t}{q_e} = \frac{1}{V_0} + \frac{t}{q_e} \quad (2)$$

where q_e is the amount of PFAS adsorbed on QNC at the equilibrium (mg g^{-1}) ($q_{e,exp}$ is the estimated value from the kinetic plot, $q_{e,cal}$ is the calculated value based on pseudo-first order), V_o is the initial sorption rate (mmol/g·h), K_1 is the pseudo-first order sorption rate constant (h^{-1}), and K_2 is the pseudo-second order sorption rate constant (g mg^{-1} h^{-1}).

A higher fitting coefficient (R^2) obtained from the pseudo-second order fitting suggested that the PFAS sorption by QNC is probably controlled by chemical sorption.[30, 31] The initial sorption rate (V_o, mmol/g·h) of the PFAS ranged from 2.2 mmol/g·h to 50.4 mmol/g·h for the PFAS examined (Table 3), i.e., two orders of magnitude higher than the reported V_o value for GAC (0.02-0.06 mmol/g·h), biochar (0.008-0.02 mmol/g·h)[28] and powdered activated carbon (PAC, 0.005-0.8 mmol/g·h).[32] The initial uptake rate during the external diffusion step is directly related

to a diffusion time constant, D/Rad^2, where D is the diffusivity of an adsorbate and Rad is the radius of the adsorbent.[33] The uptake of PFAS is expected to increase rapidly with decreasing adsorbent radius. It has been previously reported that GAC with 0.85–1.0 mm size could reach the equilibrium from 48 to 240 hr, while PAC with 45-150 um size could reach the equilibrium within 2 h.[32] As the average nanocellulose fiber dimensions were 110 ± 57 nm in length and 6.5 ± 1.4 nm in width (Figure 2), it is not surprising to observe that QNC exhibited very fast initial PFAS sorption rates and very short equilibrium time for all chosen PFAS as shown in Figure 3. The nanoscale structure of QNC provides a ~~much~~ very efficient PFAS sorption process (equilibrium within several minutes) when compared to conventional carbon-based adsorbents.

Additionally, the intra-particle diffusion model was also used to fit the kinetic data (Figure 3), where the results are listed in Table 3. This model was based on the commonly adopted diffusion process, which has the following expression:[28]

$$q_t = k_p \times t^{0.5} \quad (3)$$

where K_p (mg g^{-1} h $^{-0.5}$) is the intra-particle diffusion rate constant. Due to the low fitting R^2 value (0.84–0.11), we felt the intra-particle model is not suitable to describe the kinetic data. This suggests the PFAS adsorption on QNC is not controlled by the intra-particle diffusion process.

The typical PFAS adsorption on general adsorbent consists of three processes: (i) external diffusion from bulk solution onto the adsorbent surface, (ii) intra-particle diffusion into the adsorbent pore, and (iii) instantaneous surface adsorption at the active sites (~~may be~~ possibly fast and negligible).[34] Unlike porous GAC, where the (ii) intra-particle diffusion process is the limiting step due to the small pore size (~1 nm), the QNC scaffold doesn't contain obvious porous structure

411 (Figure 2). From both Figure 3 and Table 3, we argue the fast PFAS adsorption on QNC is very
412 likely controlled by the (i) external diffusion process, which is supported by the high initial rate V_0
413 result. Therefore, the molecular size or steric effect of PFAS has less influence on the adsorption,
414 where the kinetics mostly rely on the strength of interaction (electrostatic interaction) between
415 PFAS and QNC. Overall, QNC showed faster kinetics for both long-chain and short-chain PFAS
416 adsorption, and the equilibrium time was much shorter than those for GAC or even ion-exchange
417 resins, which usually are in the order of several days.[28, 35]

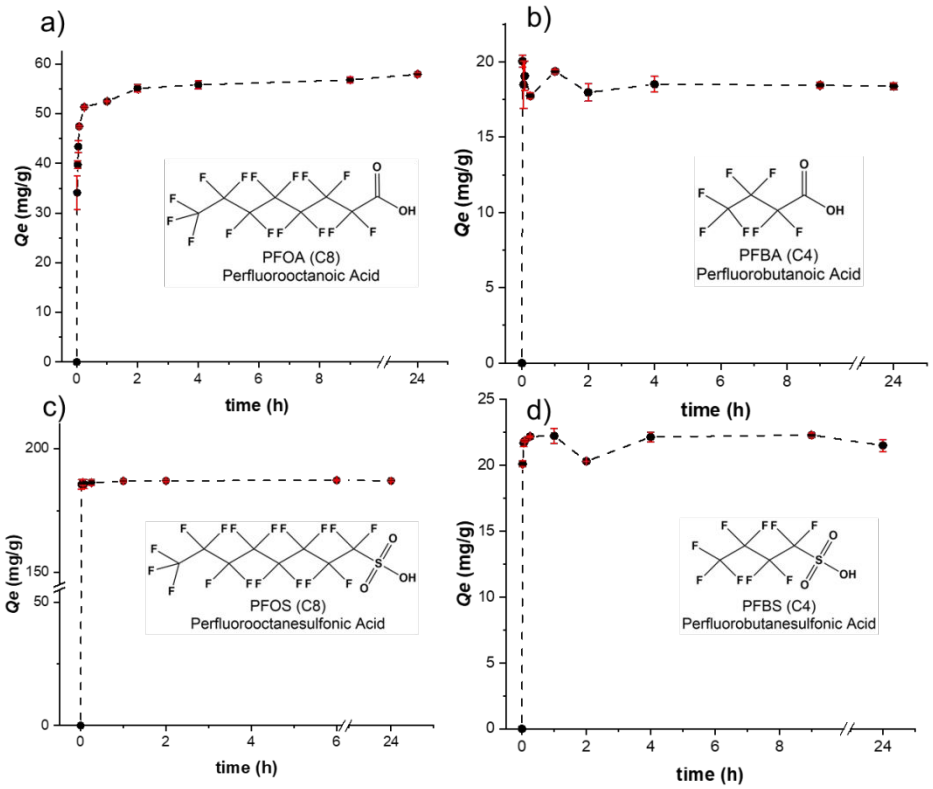

418

419 **Figure 3.** The adsorption kinetic data of QNC gel against the removal of (a) PFOA; (b) PFBA;
420 (c) PFOS; (d) PFBS over 24 hr. The error bar was calculated from two replicates. The QNC
421 concentration used was 32 mg/L for PFOA (2 mg/L) and PFOS (5 mg/L) or 320 mg/L for PFBA
422 (10 mg/L) and PFBS (10 mg/L).

423
424 **Table 3**. Pseudo-first order, pseudo-second order and intraparticle diffusion model fitting
425 parameters from the kinetic adsorption data of QNC against different PFAS compounds.

	Pseudo- first order model			Pseudo- second order model				Intraparticle diffusion model	
	$q_{e,\,cal}$ (mg/g)	K_1 (h^{-1})	R^2	q_e (mg/g)	V_0 (mmol/g· h)	K_2 (g/mg· h)	R^2	K_p ($mg \cdot g^{-1} \cdot h^{-0.5}$)	R^2
PFOA	10.96	0.29	0.70	57.97	2.2	0.27	0.99	51	0.84
PFBA	N.A.	N.A.	N.A.	19.42	15.69	8.84	0.99	18	N.A.
PFOS	1.25	1.04	0.84	187.3	50.4	7.17	0.99	186	0.78
PFBS	N.A.	N.A.	N.A.	22.29	2.64	1.60	0.99	21	0.11

426 N.A. means it is not applicable. The data can't be fitted by the model due to the large fluctuation.

427

428 **3.2.2. Adsorption Isotherm**

429

430 To observe the adsorption capacity of QNC for different PFASs, isotherm study is shown
431 in Figure 4 (also Tables S6 (a)-(d), *Supporting Information*). PFOS exhibited the highest
432 equilibrium adsorption capacity (Q_e) of 550 mg/g (1.1 mmol/g), followed by PFOA of 400 mg/g
433 (0.97 mmol/g). It is well known that sulfonic acid is a stronger acid compared with carboxylic
434 acid. Upon dissociation, the sulfonate group would exhibit a stronger anionic inductive effect than
435 the carboxylate group. Also, a DFT modeling study has been carried out, where the results
436 indicated that sulfonated PFAS has more negative exergonic energy than carboxylated PFAS.[36] As
437 a result, sulfonated PFAS could create stronger electrostatic interaction with cationic QNC than
438 carboxylated PFAS.[37] Additionally, PFOS (also PFBS) has one additional carbon in its

hydrophobic tail than PFOA (and PFBA), which may further increase its hydrophobic interaction with QNC. The combined effect of electrostatic and hydrophobic interactions between PFOS and QNC resulted in the highest Q_e value. Compared to long-chain PFOA/PFOS, short-chain PFAS exhibited a lower equilibrium adsorption capacity: PFBS of 250 mg/g (0.83 mmol/g) and PFBA of 100 mg/g (0.46 mmol/g). The above adsorption behavior is consistent with two published studies.[3, 38] A recent study [39] indicated that the higher adsorption capacity for long-chain PFAS could be due to its micelle formation, depending on the critical micelle concentrations, which is also possible in our case.

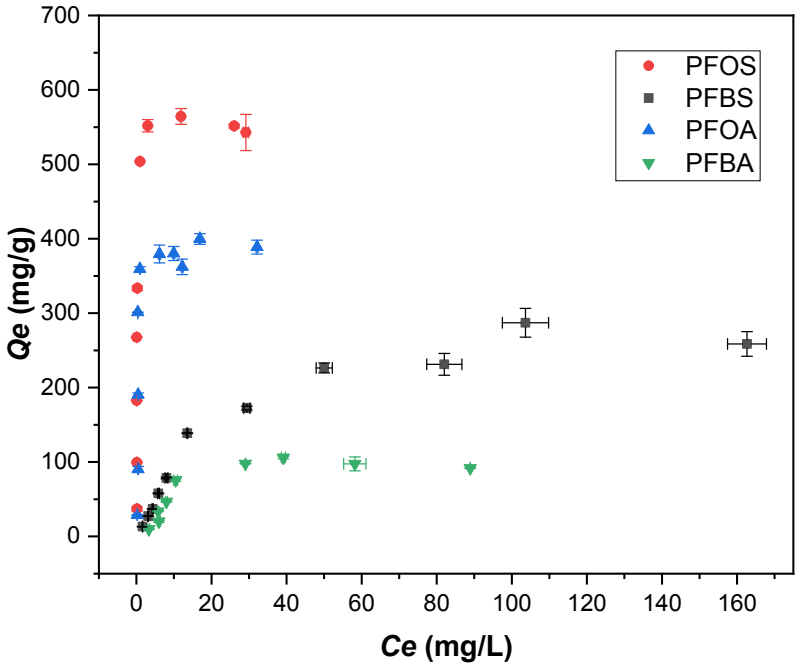

Figure 4. Equilibrium adsorption capacity (Q_e) of the QNC 12:1 adsorbent *versus* equilibrium concentration (C_e) for four different PFAS (PFAS concentration: 1-50 mg/L for PFOA and PFOS, 1- 100 mg/L for PFBA, 1- 200 mg/L for PFBS; QNC concentration: 32 mg/L for PFOA and PFOS or 320 mg/L for PFBA and PFBS; equilibrium time; 24 hr).

In the study by Giles et al, they demonstrated that the isotherm data can be described as either the sigmoidal-shaped (S), Langmuir (L), high affinity (H), or constant partition © curve, depending on the initial slope and the curvature of the isotherm data.[40] Both long-chain PFOS and PFOA isotherm data in Figure 4 followed the H-curve, as they exhibited a sharp initial slope. In contrast, short-chain PFBS and PFBA isotherm data follow the L-curve having a less steep slope and a clear plateau value. The difference could be explained by the high affinity between long-chain PFAS and QNC as compared to short-chain PFAS and QNC. To quantitatively analyze the maximum adsorption capacity of QNC against PFAS, we used the common Langmuir (Eq. 4) and Freundlich (Eq. 5) models with the following expressions to fit the results in Figure 4.

$$\frac{C_e}{Q_e} = \frac{1}{Q_m K_L} + \frac{C_e}{Q_m} \quad (4)$$

$$\log Q_e = \log K_F + \frac{1}{\mathrm{n}} \log C_e \quad (5)$$

where C_e is the equilibrium concentration of PFAS in mg/L, Q_e is the adsorbed PFAS amount (mg/g) at the equilibrium, Q_m (mg/g) represents the maximum Langmuir adsorption capacity, the Langmuir adsorption constant K_L (L/g) is positively related to the affinity of adsorption sites.[30] In the Freundlich model, the Freundlich adsorption constant K_F ($L^{1/n} \cdot mg^{1-1/n} \cdot g^{-1}$) indicates the adsorption capacity, where the n value affects the shape of curve.[30] The Langmuir model assumes the adsorption takes place on the surface as homogeneously mediated monolayer, where the Freundlich model assumes the adsorption takes place on the surface as heterogeneously mediated multi-layer. The fitting parameters of the isotherm data using these two models are summarized in Table 4.

475 **Table 4**. Langmuir and Freundlich model fitting parameters for different PFAS compounds

	Langmuir model			Freundlich model		
	Q_m (mg/g)	K_L (L/g)	R^2	K_F ($L^{1/n}\cdot mg^{1-1/n}\cdot g^{-1}$)	n	R^2
PFOA	405	1.08	0.99	174	3.09	0.42
PFBA	121	0.058	0.85	9.34	1.63	0.69
PFOS	559	2.24	0.99	290	3.66	0.39
PFBS	319	0.037	0.97	15.67	1.56	0.90

476 *The Q_m values from the Langmuir model were examined with the estimated highest Q_e values,
477 where the difference was less than 10% making the result acceptable.
478

479 The fitting results by the Langmuir model showed a very good correlation (R^2 = 0.85–0.99)
480 for all four PFASs, while the fitting by the Freundlich model was relatively poor (R^2 = 0.39-0.90).
481 To verify that there is a statistically significant difference between these two models, the one-tailed
482 paired student T-test for R^2 values was carried out ($p \leq 0.05$ means there is a statistically significant
483 difference). The results showed that QNC has the highest Q_m (559 mg/g) and K_L values (2.24 L/g)
484 for PFOS, but relatively lower Q_m (405 mg/g) and K_L values (1.08 L/g) for PFOA. However, both
485 Q_m values are considerably higher than the maximum adsorption capacity reported for GAC (236–
486 480 mg/g against PFOS and 112–195 mg/g against PFOA).[41, 42] On the other hand, the Q_m value
487 for PFBS is 319 mg/g and for PFBA is only 121 mg/g. However, these values are still higher than
488 those of conventional GAC for short-chain PFASs (e.g., 9.3-98.7 mg/g for PFBS and 5.1-51.4
489 mg/g for PFBA) and ion-exchange resins (34.6-109.2 mg/g for PFBS; 19.1-52.3 mg/g for PFBA).[28,
490 35, 41, 42] The K_L values for PFBA (0.0058 L/g) and PFBS (0.0037 L/g) are also much lower than
491 those for long-chain PFASs, confirming our notion that the adsorption affinity of short-chain PFAS

492 by QNC is less than that of long-chain PFAS by QNC.

493

494 **3.2.3. Competition adsorption studies**

495

496 Studying the competitive adsorption behavior between different types of PFAS towards
497 QNC is critical for their effective removal. We performed two experiments to understand the
498 competitive behavior among different PFASs: displacement study and competition study, where
499 the results are displayed in Figure 5 (also Tables S7 (a)-(b) for the displacement study, and Tables
500 S8 (a)-(b) for the competition study, *Supporting Information*). In the displacement study, QNC
501 was first saturated with short-chain PFAS, then long-chain PFAS was added after equilibrium. In
502 the competition study, QNC was directly exposed to the mixture of long-chain and short-chain
503 PFASs at the same concentration. We note that some previous studies were made to investigate
504 the competitive adsorption between long-chain and short-chain PFASs in anion-exchange resins.[43,
505 44] These studies indicated that the increased pH value or increased PFAS concentration could
506 induce short-chain PFAS replacement by long-chain PFAS,[44] where the displacement trend
507 depends on the PFAS molecular structure and its hydrophobicity (e.g., PFOS > PFHxS > PFOA
508 > PFBS > PFHxA > PFBA).[43] Similar competition studies for bioadsorbents are seldom reported.

509

510 Due to the high adsorption capacity in QNC, the competitive phenomenon was not obvious
511 at first when we used low concentration (10 mg/L) (Figure 5e). After increasing the initial
512 concentration gradually to 30 and 60 mg/L, the displacement behavior was seen, where the
513 percentage of the Q_e decrease in short-chain PFAS became apparent. Specifically, when the
514 displacement study was conducted at the condition of 160 mg/L QNC with ~ 60 mg/L of PFAS,

515 Q_e of PFBA decreased by 57% (from 128 mg/g to 55 mg/g) after the introduction of PFOA (Figure
516 5a). Similarly, the Q_e value of PFBS dropped by 65% (from 204 mg/g to 72 mg/g) after PFOS was
517 introduced (Figure 5b). The whole displacement process happened within 5 min for the
518 PFBS/PFOS system, where a slower equilibrium time (between 1 and 6 h) was observed for the
519 PFBA/PFOA system.
520
521 The competition study also exhibited similar behavior when we mixed long-chain and
522 short-chain PFASs simultaneously in the bisolute system. By comparing the results from single
523 solute and bisolute systems in Figure 5d, the Q_e value of bisolute PFBS was much lower than that
524 of single solute PFBS, while those of PFOS in bisolute and single solute systems remained the
525 same. A similar trend was also discovered in the PFBA/PFOA mixture (Figure 5c), but the Q_e
526 difference of PFBA was much smaller than that of PFBS. Additionally, the Q_e value of PFOA was
527 found to decrease slightly in bisolute system (Figure 5f). Based on the above results, we conclude
528 that long-chain PFAS is more easily adsorbed by QNC due to the combined electrostatic and
529 hydrophobic interactions, whereas electrostatic interaction is the dominant mechanism for short-
530 chain PFAS adsorption. Under this scenario, the displacement percentage is QNC concentration
531 dependent due to the availability of adsorption sites. These results indicate the challenge in short-
532 chain PFAS removal was due to two reasons: (i) short-chain PFAS has much lower Q_m than long-
533 chain PFAS because it lacks the hydrophobic aggregation ability; and (ii) once the adsorption
534 reaches the limit, the adsorbed short-chain PFAS can be quickly displaced by long-chain PFAS.
535

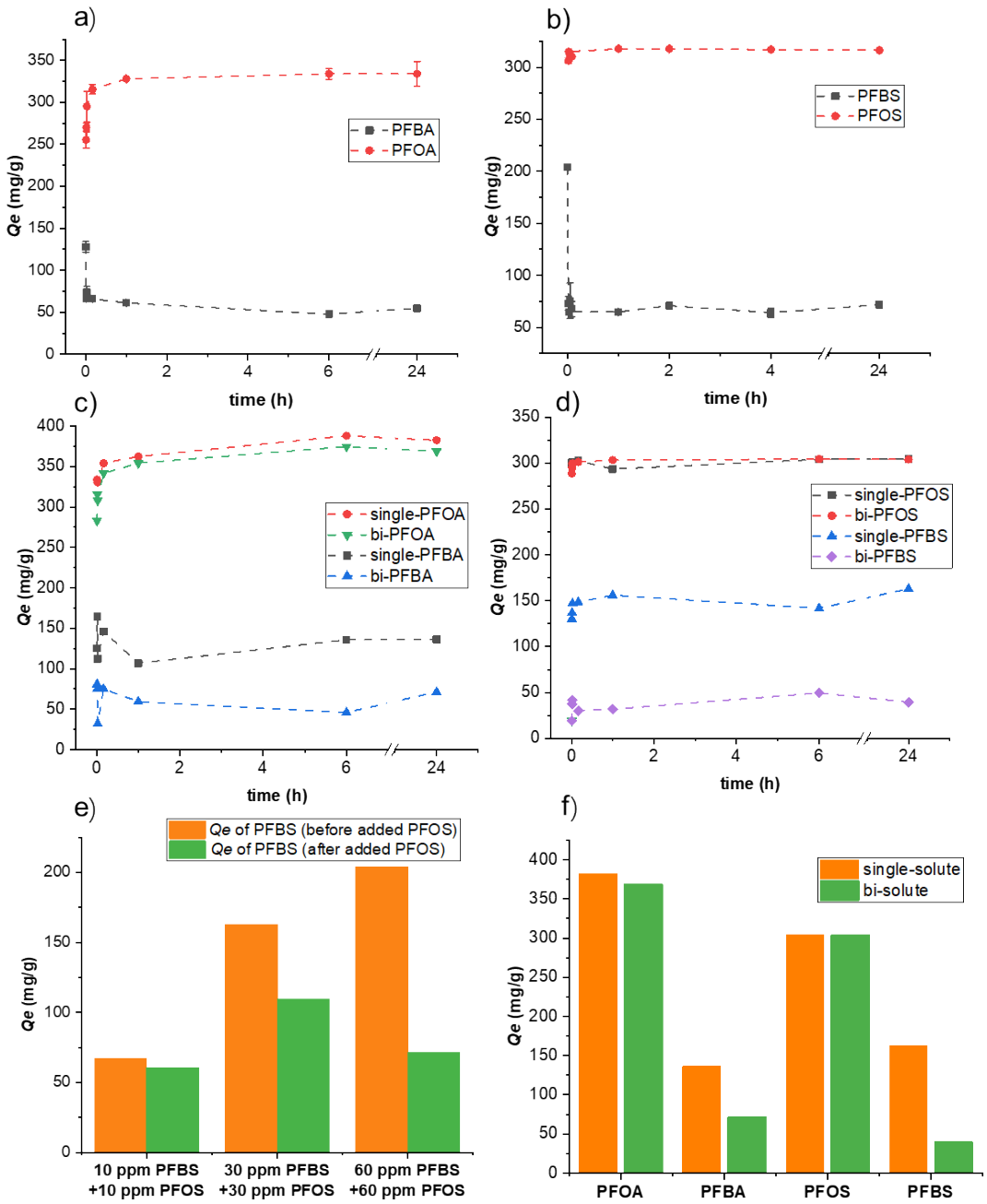

Figure 5. The Q_e versus t plots in the displacement study of (a) PFBA-PFOA/ and (b) PFBS-PFOS. (Short-chain PFAS was firstly mixed with QNC and reached equilibrium after 24 hr, and then long-chain PFAS was added into the system. The time was recorded once the long-chain PFAS was introduced. The initial PFAS concentration was 60 mg/L, QNC concentration was

541 160 mg/L). The competition adsorption studies with single solute and bisolute matrix for (c)
542 PFOA/PFBA and (d) PFOS/PFBS. (A mixture of long-chain and short-chain PFASs was added
543 to QNC at the same time. The initial PFAS concentration was 60 mg/L, QNC concentration was
544 160 mg/L). (e) The histogram comparing the Q_e values at different PFAS concentrations in the
545 displacement studies. (f) The histogram comparing the Q_e values for different PFAS in the
546 competition studies.
547
548 Additionally, the following study was carried out to understand the PFAS selectivity by QNC
549 and the competitive influence in the presence of background anions. In this study, NaCl was
550 selected as the representative salt at extremely high level (0.1 M) under an environmental relevant
551 concentration (1 mM) (Figure S4, Table S9, *supporting information*). It was surprising to observe
552 that the PFOS adsorption was not impacted by the presence of high concentration of Cl^- ions at 0.1
553 M. There are few possible explanations for this observation. (1) Since PFOS has the highest
554 hydrophobicity among four tested PFASs, it tends to form micelle or hemi-micelle with higher
555 adsorption capacity. (2) High NaCl concentration could lead to salting-out effect, resulting in lower
556 solubility for PFOS and thus better removal efficiency. (3) The electrostatic strength between
557 PFOS and quaternary ammonium group on QNC is stronger than that with chloride ions. However,
558 the removals of PFOA, PFBS and PFBA were found to decrease in the presence of anions, where
559 the Q_e of PFBA and PFBS even dropped to zero at 0.1 M of NaCl. Based on these results, we can
560 conclude that the removal of short-chain PFASs are mostly via electrostatic adsorption process
561 and are very sensitive to the background ions. In contrast, PFOS has the highest adsorption affinity
562 with minimum impact in the presence NaCl.
563

564 **3.3. Applications of QNC to Treat PFAS-Contaminated Groundwater**

565

566 To mimic the practical water treatment environment, contaminated groundwater sample
567 was collected from Long Island, NY (Table S1, *Supporting Information*) and used to evaluate the
568 effectiveness of QNC for PFAS removal. The results are shown in Table S2 (*Supporting*
569 *Information*). It was seen that the chosen groundwater sample contained 13 PFASs with total PFAS
570 concentration of 11.7 μg/L, in addition to various background ions and organics. In the QNC
571 application study, we varied the amount of QNC adsorbent to remediate the PFAS level of the
572 ground water sample for 1 h. A wood pulp sample without modification was also tested, where it
573 did not exhibit any PFAS removal capability to treat this groundwater. In Table S2, the bold
574 numbers represent the final PFAS concentration that is below the detection limit (0.01 μg/L) of
575 the LC-MS/MS instrument, and those calculated results might be underestimated.

576

577 Overall, QNC showed excellent removal efficiencies (nearly 99%) for long-chain PFASs
578 (C7-C8) even at a low adsorbent concentration (32 mg/L) (Figure 6). However, QNC only
579 displayed moderate removal efficiencies (10–60 %) for shorter chain-length PFASs (C4-C6),
580 where their removal performance increased with the increasing adsorbent dose. For example, the
581 removal percentage of perfluoropentane sulfonic acid (PFPeS) and perfluoroheptanoic acid
582 (PFHpA) reached >90% at 640 mg/L of QNC, while the removal of PFBS, 4:2 fluorotelomer
583 sulfonic acid (4:2 FTS) and PFHxA reached only ~50% at the same QNC dose (640 mg/L). It was
584 found that short-chain carboxylated PFAS, such as PFBA and PFPeA, were the most difficult
585 components to be removed (< 10%) even at the highest QNC concentration (640 mg/L). This may
586 be due to their low adsorption affinity (carboxylate group) towards the QNC, combined with the

587 interference effects (i.e., displacement and competition) between varying PFASs and other co-
588 constituents (inorganic anions etc.) in groundwater. Another observation is that for PFASs with
589 the same carbon number, sulfonate PFASs always showed better affinity to QNC than carboxylate
590 PFASs (e.g., C-F 4 compounds removal, PFBS 13-51% and PFPeA 2-8%; C-F 5 compounds
591 removal, PFPeS 51-93% and PFHxA 17-49%). In addition, in the C-F 4 compound group, there is
592 no significant removal difference between PFBS (13-51%) and 4:2 FTS (14-53%) ($P > 0.05$ in the
593 T-test), indicating the influence of functional group is more profoundly than the influence of chain-
594 length in this system. The overall adsorption trend is similar to other studies which also point out
595 the challenge of PFBA removal.[36, 45, 46]

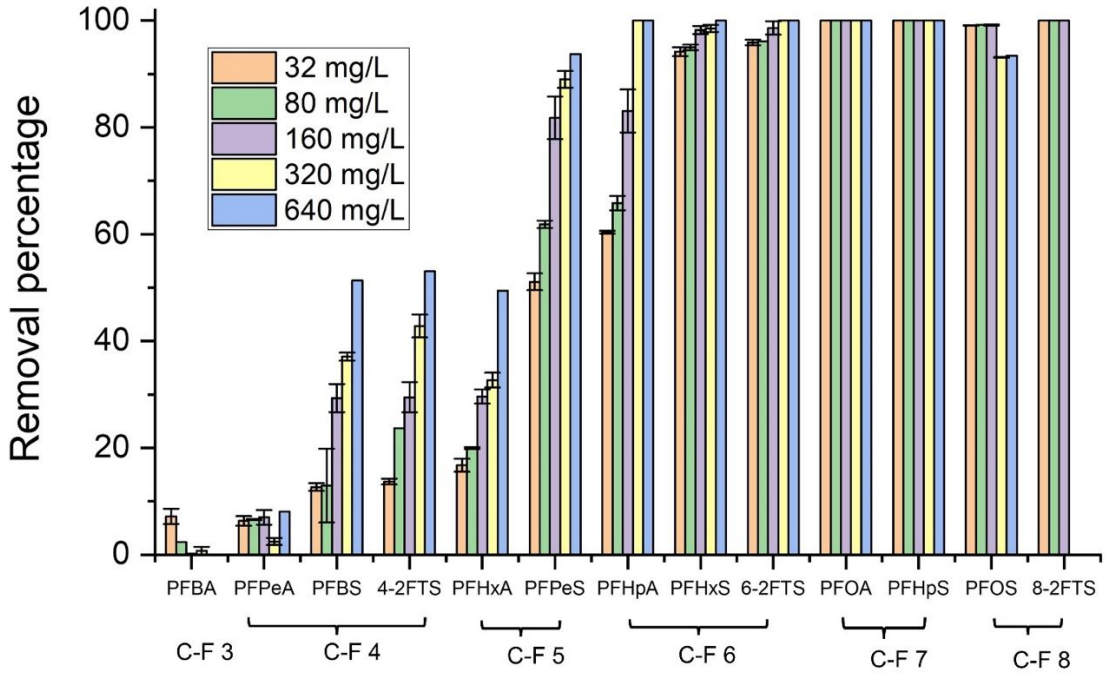

596

597 **Figure 6.** Removal percentage of different PFASs in ground water sample by using various
598 amounts of QNC (experimental condition: 9 ml ground water was mixed with 1 ml of QNC gel
599 at 0.0032 – 0.064 wt% for 1 hr).

600

601 **4. PFAS Removal Mechanism by QNC**

602

603 To-date, there are a great deal of studies regarding the PFAS removal mechanism, and it is
604 well known that electrostatic interaction (ionic bonding) is much stronger than hydrophobic
605 interactions (noncovalent bonding).[14, 15] The electrostatic interaction as the dominant PFAS
606 removal mechanism has been reported in some cationic amine-containing organic adsorbents,
607 which also exhibited the rapid PFAS removal kinetics.[19, 20, 36, 47, 48] Park et al. investigated the
608 PFAS removal performance in magnetic ion-exchange resins to understand the role of the charge
609 interaction.[37] Surprisingly, PFOS and its branched isomer with different hydrophobicity showed
610 almost equal equilibrium uptake due to their similar total atomic charge.[49] The results clearly
611 indicate that electrostatic interaction is the dominant force in the chosen magnetic ion-exchange
612 resin system, where the role of hydrophobic interaction is minor.[37]

613

614 As the QNC system in this study possesses plenty of cationic charged groups on surface so
615 that electrostatic removal can be considered as primary driving force. However, the higher removal
616 capacity for long-chain PFAS removal in isotherm study indicated that the hydrophobic attraction
617 (due to van der Wall forces) also plays an important role. The results from the
618 competition/displacement studies and the ground water test clearly indicate that long-chain PFASs
619 have better adsorption affinity than short-chain PFASs towards the QNC adsorbent due to
620 additional hydrophobic interaction. The ion test confirmed that short-chain PFASs are easily
621 affected by the presence of other anions as their dominant mechanism is electrostatic adsorption.
622 In the groundwater test containing multiple PFAS mixtures, the PFBA removal capacity was the
623 lowest, indicating that electrostatic attraction between the carboxylate group in PFAS and

ammonium group on QNC was lower than that between the sulfonate group in PFAS and QNC.

The maximum adsorption capacity Q_m in the molar unit mmol/g (instead of the weight unit mg/g) is an important measure to understand the removal mechanism, as the value reflects the amount of the functional group on QNC. According to the conductivity titration result in Table 1, the amount of quaternary ammonium group (NR_4^+) is 0.486 mmol/g for the tested QNC adsorbent (QNC 12:1). It is surprising to notice that PFOS (1.12 mmol/g), PFBS (1.06 mmol/g) and PFOA (0.98 mmol/g) showed similar Q_m values in the molar unit, which is close to 1.0 mmol/g or about a 2:1 ratio when compared to the content of NR_4^+ group (Table 5). However, Q_m of PFBA is only 0.57 mmol/g, which is 1:1 to the NR_4^+ group and indicates that the adsorption is mainly by electrostatic attraction between the two. One recent study of ion-exchange resin IRA 910 showed similar results, where adsorbed PFAS and released chloride ratio was measured to elucidate the adsorption mechanism for each PFAS.[43] The PFBA with chloride ratio was found to be 1, while all other long-chain PFASs exhibited a ratio larger than 1.[43] Since PFBS, PFOA and PFBS are more hydrophobic than PFBA, we hypothesize that the hydrophobic interaction between PFAS molecules, forming a dimer or small aggregation (e.g. hemi-micelle) structure with one PFAS molecule tethered to the QNC backbone, may be a possible pathway to enhance the adsorption capacity. The proposed mechanism is shown in Figure 7. Unfortunately, we do not have any further experimental results (such as scattering) to support this hypothesis. When comparing PFOA and PFBS, the effect of functional group might offset the effect of chain-length (PFOA: longer chain and weaker functional group: PFBS: shorter chain but stronger functional group), thus yielding the similar adsorption capacity. This phenomenon also indicates that in the electrostatic interaction driven system like QNC, the role of functional groups on PFAS weighs more than the role of

647 hydrophobicity affecting the adsorption capacity. This hypothesis is also supported by the
648 groundwater result. As PFBA has the lowest hydrophobicity and lowest electrostatic affinity
649 among four tested PFASs, PFBA showed the lowest adsorption capacity by QNC since it can only
650 be removed by electrostatic interaction.[36, 48] Nevertheless, Q_m of PFBA on QNC (121 mg/g) is still
651 higher than most of non-charged adsorbents such as GAC and biochar (5.1-51.36 mg/g) (Table 5),
652 supporting that electrostatic interaction is beneficial to short-chain PFAS removal.

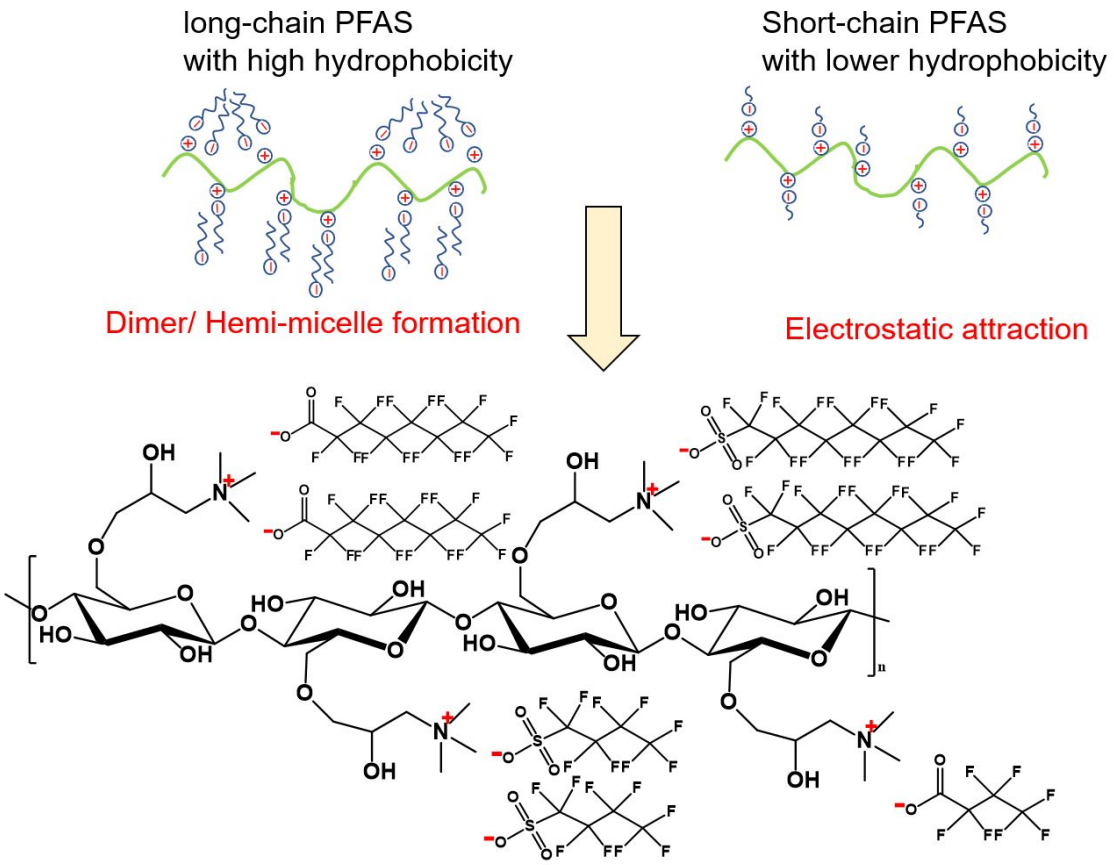

653
654 **Figure 7.** The proposed adsorption mechanism of long-chain and short-chain PFASs by the QNC
655 adsorbent.
656
657 In addition to evaluating the maximum adsorption capacity, we have also compared the
658 molar ratio of Q_m (close to Q_e) between short-chain (C4) and long-chain (C8) PFASs using

different adsorbents in the relevant studies, where the results are summarized in Table 5. In this table, the Q_m molar ratio can provide the benchmark to evaluate the short-chain PFAS adsorption capacity for each adsorbent relative to their long-chain analogues. In principle, the available adsorption sites on the adsorbent are fixed, so the difference in the removal capacity for each PFAS compound is only related to their sorption affinity. The higher molar ratio of Q_m between short-chain and long-chain PFAS indicates that the sorption affinity between the two becomes more similar. As seen in Table 5, the maximum adsorption capacity of short-chain PFASs are rarely reported to surpass their long-chain counterparts. However, the Q_m molar ratio of short-chain/long-chain PFASs can often reach close to 0.7 – 0.9 as a good standard.[43] There are some exceptions for organically modified silica and exchange resin (IRA 910), whose PFBS/PFOS ratio is larger than 1.0. This may be because the Q_m in the silica study was too low, and the correlation of the Langmuir model for PFOS in the IRA 910 study was poor (R^2 = 0.71), rendering the calculated ratio values unreliable.

In Table 5, the chosen adsorbents can be classified into three categories: synthetic materials (containing bioadsorbents), carbonaceous materials, and ion-exchange resins. In synthetic materials, the corresponding Q_m mole ratios of short-chain/long-chain PFASs are relatively high. For example, aminated rice husk shows high Q_m values for both long-chain and short-chain PFASs, leading to a Q_m molar ratio of PFBA/PFOA ~~as~~ of 0.68. This can be attributed to the abundant cationic charge groups on the adsorbent surface.[39] Our current study yielded results similar to the study of aminated rice husk: the Q_m molar ratio of PFBA/PFOA only reached 0.58, while that of PFBS/PFOS was 0.95, suggesting that the sorption affinity in short-chain sulfonated PFBS was also high. Zirconium-based metal-organic framework (NU-1000) was another

successful example that used electrostatic interactions to remove PFAS effectively.[49] The adsorbent showed similar removal for both long-chain and short-chain PFAS (adsorption molar ratio was ~1.0), and the primary adsorption mechanism was anion exchange reaction at the metal node. For GAC and biochar materials, their Q_m values are moderate for long-chain PFAS but relatively low for short-chain PFAS (PFBA and PFBS), resulting in low Q_m molar ratios of short-chain PFAS versus long-chain PFAS. This result can be expected because the hydrophobic interaction is the major mechanism in activated carbons, where the adsorption and process of short-chain PFAS aggregation becomes unlikely due to the reduced hydrophobicity. In the case of ion-exchange resins, the Q_m molar ratios of short-chain/long-chain PFAS varied and did not show a clear trend. Perhaps this is because its Q_m value is strongly influenced by the polymeric backbone and available functional groups. For instance, Zaggia et al. compared three ion-exchange resins with different hydrophobicity, and it was found that the resin A532E with more hydrophobic functional groups exhibited higher adsorption capacity for both long-chain and short-chain PFAS than A520E (fairly hydrophobic) and A600E (non-hydrophobic). The increased hydrophobicity in A532E led to a high Q_m value for short-chain PFAS adsorption, rendering higher Q_m molar ratios of short-chain/long-chain PFAS (0.72 for PFBA/PFOA and 0.69 for PFBS/PFOS).[35] In the case of IRA 910, an ion-exchange resin containing polystyrene-divinylbenzene backbone and dimethyl ethanol ammonium group, it showed very high Q_m values for all four PFASs yielding a high Q_m molar ratio of short-chain/long-chain PFAS (0.86 for PFBA/PFOA).[43] Based on the results from Table 5, we conclude that synthetic materials with high charge density and ion-exchange resins are more effective than carbonaceous materials for short-chain PFAS removal, due to higher electrostatic interactions between PFAS and adsorbent.

705 **Table 5**. Summary and comparison of the maximum adsorption capacity and the molar ratio of

706 short-chain/long-chain PFAS in relevant studies.

Adsorbent	**Experimental condition**	**PFOA Q_m**	**PFBA Q_m**	**Q_m molar ratio PFBA/ PFOA**	**PFOS Q_m**	**PFBS Q_m**	**Q_m molar ratio PFBS/ PFOS**	**Ref**
Synthetic materials								
quaternized nanocellulose (QNC)	adsorbent dose = 32 mg/L (PFOA and PFOS) or 320 mg/L (PFBA and PFBS); Co = 1-50 mg/L (PFOA and PFOS), 1- 100 mg/L (PFBA), 1-250 mg/L (PFBS)	405 mg/g (0.98 mmol/g)	121 mg/g (0.57 mmol/g)	0.58	559 mg/g (1.12 mmol/g)	319 mg/g (1.06 mmol/g)	0.95	Our work
Aminated rice husk	adsorbent dose = 100 mg/L; Co = 0 - 0.5 mmol/L	1031 mg/g (2.49 mmol/g)	364 mg/g (1.7 mmol/g)	0.68	1325 mg/g (2.65 mmol/g)	N.A.	N.A.	[39]
Covalent triazine-based framework	adsorbent dose = 250 mg/L; 3.8 -259 mg/L (PFOA), 59.9 - 415 mg/L (PFOS), 6.5- 204 mg/L (PFBA), 6-247 mg/L (PFBS)	269 mg/g (0.65 mmol/g)	92 mg/g (0.43 mmol/g)	0.66	665 mg/g (1.33 mmol/g)	141 mg/g (0.47 mmol/g)	0.35	[41]
Organically modified silica (poly-SOMS)	adsorbent dose = 40 mg/L; Co = 0.25-2 mg/L	12.7 mg/g (0.031 mmol/g) [1]	5.7 mg/g (0.027 mmol/g) [1]	0.87	8.9 mg/g (0.018 mmol/g) [1]	7.7 mg/g (0.026 mmol/g) [1]	1.44	[27]
Zirconium-based metal-organic framework	adsorbent dose = 200 mg/L; Co = 100 mg/L	507 mg/g (1.22 mmol/g)	274 mg/g (1.28 mmol/g)	1.05	622 mg/g (1.24 mmol/g)	404 mg/g (1.35 mmol/g)	1.09	[49]
Carbonaceous materials								
AC Calgon	adsorbent dose = 250 mg/L; 3.8 -259 mg/L (PFOA), 59.9 - 415 mg/L (PFOS), 6.5- 204 mg/L (PFBA), 6-247 mg/L (PFBS)	195 mg/g (0.47 mmol/g)	51.36 mg/g (0.24 mmol/g)	0.51	480 mg/g (0.96 mmol/g)	51 mg/g (0.17 mmol/g)	0.18	[41]

GAC Calgon 400	adsorbent dose = 1000 mg/L; Co = 15- 150 mg/L	112.1 mg/g (0.27 mmol/g)	N.A.	N.A.	236.4 mg/g (0.47 mmol/g)	98.7 mg/g (0.33 mmol/g)	0.70	[42]
GAC Calgon F-600	adsorbent dose = 20- 2000 mg/L; Co = 50 mg/L	76.1 mg/g (0.18 mmol/g)[2]	15.3 mg/g (0.071 mmol/g)[2]	0.39	81.3 mg/g (0.16 mmol/g)[2]	40 mg/g (0.13 mmol/g)[2]	0.81	50
GAC	adsorbent dose = 50 mg/L; Co = 0.1- 1 mg/L	35.6 mg/g (0.086 mmol/g)	5.1 mg/g (0.024 mmol/g)	0.28	60 mg/g (0.12 mmol/g)	9.3 mg/g (0.031 mmol/g)	0.26	[28]
Biochar	adsorbent dose = 50 mg/L; Co = 0.1- 1 mg/L	21.5 mg/g (0.052 mmol/g)	10.3 mg/g (0.048 mmol/g)	0.92	35 mg/g (0.070 mmol/g)	6.9 mg/g (0.023 mmol/g)	0.33	[28]
Ion-exchange resins								
IRA 910	adsorbent dose = 100 mg/L; Co = 50- 400 mg/L	1436.6 mg/g (3.47 mmol/g)	635.7 mg/g (2.97 mmol/g)	0.86	1395 mg/g (2.79 mmol/g)[3]	1023.3 mg/g (3.41 mmol/g)	1.22	[43]
A600E	adsorbent dose = 1000 mg/L; Co = 1000 mg/L	125.2 mg/g (0.30 mmol/g)[4]	19.1 mg/g (0.089 mmol/g)[4]	0.30	186.2 mg/g (0.37 mmol/g)[4]	34.6 mg/g (0.12 mmol/g)[4]	0.32	[35]
A520E	adsorbent dose = 1000 mg/L; Co = 1000 mg/L	134.7 mg/g (0.33 mmol/g)[4]	29.5 mg/g (0.14 mmol/g)[4]	0.42	210.4 mg/g (0.42 mmol/g)[4]	53.8 mg/g (0.18 mmol/g)[4]	0.43	[35]
A532E	adsorbent dose = 1000 mg/L; Co = 1000 mg/L	142.1 mg/g (0.34 mmol/g)[4]	52.3 mg/g (0.24 mmol/g)[4]	0.72	260.5 mg/g (0.52 mmol/g)[4]	109.2 mg/g (0.36 mmol/g)[4]	0.69	[35]

N.A. means there is no data available for specific PFAS.
The Q_{max} values are derived from Langmuir fitting result, unless otherwise noted.
[1] The Q_e value was calculated at C_e= 200 μg/L using the Freundlich fitting model
[2] The Q_{max} value was estimated from the BET isotherm model
[3] The Langmuir correlation (R^2 = 0.71) was poor for PFOS in IRA 910
[4] The Q_e value was estimated based on the adsorption curve at the equilibrium

5. Conclusions

The current study demonstrates the development of a cationic quaternized nanocellulose (QNC) adsorbent system, which is potentially low cost, sustainable and effective to remove a wide range of long-chain and short-chain PFAS molecules. This is because the availability of abundant cationic sites (quaternary ammonium groups) and the large surface area in QNC facilitate both

720 electrostatic and hydrophobic interactions with anionic PFAS molecules, resulting in fast removal
721 kinetics and high removal capacity. The major findings can be summarized as below:
722
723 I. From the adsorption isotherm study, the calculated maximum adsorption capacity results
724 (expressed in the molar unit) indicate that the adsorbed long-chain PFAS molecules may
725 induce a dimer or small aggregation (hemi-micelle) structure with other PFAS molecules,
726 resulting in higher values. In contrast, the maximum adsorption capacity of PFBA and the
727 results from the NaCl ion test indicate that electrostatic interaction is the only driving force for
728 the adsorption of PFBA onto the cationic sites in QNC.
729 II. Both displacement and competition studies indicate that short-chain PFASs could be easily
730 displaced by their long-chain counterparts, where the competitive level is also dependent on
731 the initial PFAS concentration.
732 III. Using a groundwater sample collected on Long Island, New York, the demonstrated QNC
733 system effectively removed most PFASs, with the exception of carboxylated short-chain
734 PFASs, such as PFBA and PFPeA.
735
736 This work demonstrated the importance of electrostatic interaction in terms of enhanced
737 short-chain PFAS removal, according to relatively higher adsorption amount and molar ratio
738 (short-chain versus long-chain) as compared to conventional GAC system. We believe the QNC
739 system can outperform most of synthetic adsorbents and ion-exchange polymers in many aspects,
740 such as sustainability and performance/cost ratio. However, the strategy to improve the removal
741 efficiency against carboxylated short-chain PFASs ($C \leq 4$) will still need to be developed to take
742 advantage of the unique nature of nanocellulose scaffolds. Some perspectives include utilized

743 synergistic effects by combining electrostatic interaction with hydrophobic or fluor-fluor
744 interactions. [27, 46, 50, 51]
745
746 In terms of practical applications, unlike conventional adsorbents, QNC itself is relatively
747 low-cost, biodegradable, and environmentally friendly[18]. As a result, the used samples can be
748 safely destroyed without the need for expensive regeneration of the adsorbent. The destruction
749 techniques may include the methods of plasma, electron beam and electrochemistry. To ensure the
750 safe handling of nanomaterials for industrial applications, post cross-linking method or
751 solidification methods can be further used to ensure the use of nanocellulose as adsorbent media.
752 QNC represents a new class of PFAS remediation material, which provides complementary
753 property when compared with other effective adsorbents (e.g., GAC, ion exchange resins, and
754 MOF). It is conceivable QNC can be used in combination with these adsorbents in a sequential
755 manner to achieve more effective PFAS removal efficiency.
756
757 **Acknowledgements**
758
759 The authors acknowledge the financial support of this work by the Division of Chemical,
760 Bioengineering, Environmental and Transport Systems (CBET- 2052772) and the Division of
761 Materials Science (DMR- 2216585) of the US National Science Foundation, and the NYS Center
762 for Clean Water Technology at Stony Brook University.
763
764

Reference

1. R. C. Buck, J. Franklin, U. Berger, J. M. Conder, I. T. Cousins, P. de Voogt, A. A. Jensen, K. Kannan, S. A. Mabury and S. P. van Leeuwen, *Integr Environ Assess Manag*, 2011, **7**, 513-541.
2. B. Kuehn, *JAMA*, 2019, **322**, 1757-1757.
3. F. Li, J. Duan, S. Tian, H. Ji, Y. Zhu, Z. Wei and D. Zhao, *Chemical Engineering Journal*, 2020, **380**, 122506.
4. O. U. G. P. Group, *Synthesis paper on per- and polyfluorinated chemicals (PFCs)*, Paris: Health and Safety Environment, Environment Directorate, 2013.
5. C. T. Vu and T. Wu, *Environmental Science: Water Research & Technology*, 2020, **6**, 2958-2972.
6. K. Loria, *Dangerous PFAS Chemicals Are in Your Food Packaging*, Consumer Reports, 2022.
7. P. Grandjean, C. A. G. Timmermann, M. Kruse, F. Nielsen, P. J. Vinholt, L. Boding, C. Heilmann and K. Mølbak, *PLoS One*, 2020, **15**, e0244815-e0244815.
8. M. Nian, K. Luo, F. Luo, R. Aimuzi, X. Huo, Q. Chen, Y. Tian and J. Zhang, *Environmental Science & Technology*, 2020, **54**, 8291-8299.
9. E. Marques, M. Pfohl, W. Wei, G. Tarantola, L. Ford, O. Amaeze, J. Alesio, S. Ryu, X. Jia, H. Zhu, G. D. Bothun and A. Slitt, *Toxicology and Applied Pharmacology*, 2022, **442**, 115991.
10. K. Londhe, C.-S. Lee, Y. Zhang, S. Grdanovska, T. Kroc, C. A. Cooper and A. K. Venkatesan, *ACS ES&T Engineering*, 2021, **1**, 827-841.
11. I. Ross, J. McDonough, J. Miles, P. Storch, P. Thelakkat Kochunarayanan, E. Kalve, J. Hurst, S. S. Dasgupta and J. Burdick, *Remediation Journal*, 2018, **28**, 101-126.
12. A. K. Venkatesan, C.-S. Lee and C. J. Gobler, *Science of The Total Environment*, 2022, **847**, 157577.
13. M. Park, S. Wu, I. J. Lopez, J. Y. Chang, T. Karanfil and S. A. Snyder, *Water Research*, 2020, **170**, 115364.
14. Z. Du, S. Deng, Y. Bei, Q. Huang, B. Wang, J. Huang and G. Yu, *J Hazard Mater*, 2014, **274**, 443-454.
15. D. Banks, B.-M. Jun, J. Heo, N. Her, C. M. Park and Y. Yoon, *Separation and Purification Technology*, 2020, **231**, 115929.
16. D. Q. Zhang, W. L. Zhang and Y. N. Liang, *Sci Total Environ*, 2019, **694**, 133606.
17. P. Ganguly, A. Breen and S. C. Pillai, *ACS Biomaterials Science & Engineering*, 2018, **4**, 2237-2275.

18. R. Das, T. Lindstrom, P. R. Sharma, K. Chi and B. S. Hsiao, *Chem Rev*, 2022, 8936–9031.
19. D. Li, K. Londhe, K. Chi, C. S. Lee, A. K. Venkatesan and B. S. Hsiao, *AWWA Water Science*, 2021, **3**, e1258.
20. J. T. Harris, G. D. de la Garza, A. M. Devlin and A. J. McNeil, *ACS ES&T Water*, 2022, **2**, 349-356.
21. H. Sehaqui, A. Mautner, U. Perez de Larraya, N. Pfenninger, P. Tingaut and T. Zimmermann, *Carbohydr Polym*, 2016, **135**, 334-340.
22. A. Pei, N. Butchosa, L. A. Berglund and Q. Zhou, *Soft Matter*, 2013, **9**, 2047.
23. S. Saini, C. Yucel Falco, M. N. Belgacem and J. Bras, *Carbohydr Polym*, 2016, **135**, 239-247.
24. M. Zaman, H. Xiao, F. Chibante and Y. Ni, *Carbohydr Polym*, 2012, **89**, 163-170.
25. B. Ivanova, T. Kolev and M. Spiteller, 2010, pp. 675-755.
26. A. R. Katritzky, *Journal of the American Chemical Society*, 1996, **118**, 3543-3543.
27. E. K. Stebel, K. A. Pike, H. Nguyen, H. A. Hartmann, M. J. Klonowski, M. G. Lawrence, R. M. Collins, C. E. Hefner and P. L. Edmiston, *Environmental Science: Water Research & Technology*, 2019, **5**, 1854-1866.
28. D. Zhang, Q. He, M. Wang, W. Zhang and Y. Liang, *Environ Technol*, 2021, **42**, 1798-1809.
29. P. McCleaf, S. Englund, A. Ostlund, K. Lindegren, K. Wiberg and L. Ahrens, *Water Res*, 2017, **120**, 77-87.
30. Q. Hu, Q. Wang, C. Feng, Z. Zhang, Z. Lei and K. Shimizu, *Journal of Molecular Liquids*, 2018, **254**, 20-25.
31. Y. S. Ho and G. McKay, *Process Biochemistry*, 1999, **34**, 451-465.
32. Y. Zhi and J. Liu, *Environ Pollut*, 2015, **202**, 168-176.
33. R. T. Yang, *Adsorbents: Fundamentals and Applications*, John Wiley & Sons, Inc., 2003.
34. P. Chingombe, B. Saha and R. J. Wakeman, *J Colloid Interface Sci*, 2006, **302**, 408-416.
35. A. Zaggia, L. Conte, L. Falletti, M. Fant and A. Chiorboli, *Water Res*, 2016, **91**, 137-146.
36. M. Ateia, M. Arifuzzaman, S. Pellizzeri, M. F. Attia, N. Tharayil, J. N. Anker and T. Karanfil, *Water Research*, 2019, **163**, 114874.
37. M. Park, K. D. Daniels, S. Wu, A. D. Ziska and S. A. Snyder, *Water Res*, 2020, **181**, 115897.
38. E. Gagliano, M. Sgroi, P. P. Falciglia, F. G. A. Vagliasindi and P. Roccaro, *Water Res*, 2020, **171**, 115381.
39. S. Deng, L. Niu, Y. Bei, B. Wang, J. Huang and G. Yu, *Chemosphere*, 2013,

91, 124-130.
40. C. H. Giles, D. Smith and A. Huitson, *Journal of Colloid and Interface Science*, 1974, **47**, 755-765.
41. B. Wang, L. S. Lee, C. Wei, H. Fu, S. Zheng, Z. Xu and D. Zhu, *Environ Pollut*, 2016, **216**, 884-892.
42. V. Ochoa-Herrera and R. Sierra-Alvarez, *Chemosphere*, 2008, **72**, 1588-1593.
43. A. Maimaiti, S. Deng, P. Meng, W. Wang, B. Wang, J. Huang, Y. Wang and G. Yu, *Chemical Engineering Journal*, 2018, **348**, 494-502.
44. W. Wang, X. Mi, Z. Zhou, S. Zhou, C. Li, X. Hu, D. Qi and S. Deng, *J Colloid Interface Sci*, 2019, **557**, 655-663.
45. H. Son, T. Kim, H.-S. Yoom, D. Zhao and B. An, *Water*, 2020, **12**.
46. X. Min and Y. Wang, *J Hazard Mater*, 2023, **449**, 131047.
47. W. Ji, L. Xiao, Y. Ling, C. Ching, M. Matsumoto, R. P. Bisbey, D. E. Helbling and W. R. Dichtel, *J Am Chem Soc*, 2018, **140**, 12677-12681.
48. E. Kumarasamy, I. M. Manning, L. B. Collins, O. Coronell and F. A. Leibfarth, *ACS Cent Sci*, 2020, **6**, 487-492.
49. R. Li, S. Alomari, R. Stanton, M. C. Wasson, T. Islamoglu, O. K. Farha, T. M. Holsen, S. M. Thagard, D. J. Trivedi and M. Wriedt, *Chemistry of Materials*, 2021, **33**, 3276-3285.
50. X. Tan, M. Sawczyk, Y. Chang, Y. Wang, A. Usman, C. Fu, P. Král, H. Peng, C. Zhang and A. K. Whittaker, *Macromolecules*, 2022, **55**, 1077-1087.
51. Q. Dong, X. Min, J. Huo and Y. Wang, *Chemical Engineering Journal Advances*, 2021, **7**, 100135.